Wavy and rough cracks in silicon

Robert D. Deegan, Shilpa Chheda, Lisa Patel, M. Marder, and Harry L. Swinney
Center for Nonlinear Dynamics and Department of Physics, The University of Texas at Austin, Austin, Texas 78712, USA

Jeehoon Kim and Alex de Lozanne
Department of Physics, The University of Texas at Austin, Austin, Texas 78712, USA
(Received 19 December 2002; published 23 June 2003)

Single-crystal silicon exhibits a strong preference to cleave along a few certain planes, but in experiments we observe wavy cracks with almost no evidence of a preferred fracture direction. Furthermore, we find that the fracture surface is an anisotropic and self-affine fractal over five decades in length scale in the direction of the crack with a roughness exponent of 0.78. In our experiments a 1–4 cm wide strip of single-crystal silicon is heated to 378 °C and lowered into a 20 °C water bath at speeds of 0.2–5 cm/s. The thermal gradient produces cracks that, depending on the speed, are straight, wavy with amplitude 0.1–0.5 cm and wavelength 0.3–1 cm, or multibranched. The transition from one mode of fracture to another is discontinuous and hysteretic.

DOI: 10.1103/PhysRevE.67.066209 PACS number(s): 89.75.Kd, 62.20.Mk, 68.35.Ct

I. INTRODUCTION

As safety margins in engineering are abbreviated in the quest for ever lighter and smaller devices, failure due to fracture is an increasing problem. The manufacturing of microelectromechanical and microfluidic devices from silicon is a case in point: the drive to miniaturization is on a collision course with the mechanical limits of silicon. Yet, fracture in single crystals is poorly understood in comparison with fracture in isotropic materials. In particular, there is no consensus on the path selection criterion for quasistatic cracks in crystals.

We present experimental results on crack path selection and fracture surface roughness in single-crystal silicon. Our experiments are based on the technique developed by Yuse and Sano [1], who showed that the shape of the crack produced when a heated strip of glass is lowered into a cold water bath undergoes a transition from straight to wavy as the dipping rate increases. A comparison of theory [2–4] and the results from that experiment and others [4–8] provides a compelling case for the "principle of local symmetry" [9], which posits that slow cracks advance such that the shear stress at and parallel to the crack tip vanishes.

For our experiments we used $\langle 100 \rangle$ single-crystal silicon wafers, which are known to cleave easily and exclusively along the $\langle 110 \rangle$ direction. We expected that the anisotropic surface energy of silicon would prevent the wavy fracture mode or at least make the oscillations jagged. Instead, we found that there is a transition from straight to wavy cracks [10], that the wavy crack appears smooth to the eye, and that the anisotropy only delays the transition. We also found that the new surface made by wavy cracks is free of facets on all scales above the 10 nm limit of our resolution. Furthermore, even though silicon wafers come moderately close to crystalline perfection, we find that the fracture surface is self-affine and has a roughness exponent equal to that seen in highly heterogeneous materials.

II. EXPERIMENT

A schematic of our experimental setup is shown in Fig. 1. A thin, narrow strip of single-crystal silicon is attached to a translation stage via an extension strip. The stage is moved by a microstepper motor which can produce linear steps of 3 μm. The silicon is lowered into an oven held at 378 °C. Other temperatures in the range 350–410 °C were also used but the results were essentially unchanged. The oven consists of two copper plates (23 cm$\times$14 cm$\times$0.9 cm) held apart by 0.6 cm thick copper spacers. A thin film heater (10 cm $\times$18 cm) is pressed into contact with the outer side of each copper plate. The temperature is monitored with a K-type thermocouple lodged in the center of one of the plates and regulated with a commercial proportional-integral-derivative temperature controller. The copper plates are insulated from the environment by several centimeters of sand. After the sample reaches thermal equilibrium with the oven, the silicon is lowered at a fixed speed into a 20 °C water bath with a minute quantity of Kodak Photoflow added to reduce surface tension.

The silicon strips are made from a 20 cm diameter, 685 μm thick, $\langle 100 \rangle$, boron-doped, 6 Ω cm wafer by cleaving along $\langle 110 \rangle$ planes. The relevant properties of silicon are given in Table I. The wafers are mechanically polished on both sides and chemically polished on one side. The resulting samples varied in length from 12.7 to 19.5 cm and in width from 1.0 to 3.5 cm. A 1 cm long seed crack is introduced by notching the surface with a diamond pen halfway between the center and the side, and loading it in a three-point bending mode. In our initial trials the samples were cleaned with a degreaser and acetone. However, we skipped this step in later trials because it did not affect the outcome.

The initial contact of the sample with the water produces a significant explosion of steam. Infrared video shows that the temperature gradient reaches steady state within seconds. Measurements of the wafer temperature with a thermocouple show that the temperature of the wafer at the point of contact with the water is pinned at 100 °C due to the vaporization of the water. Water is drawn by capillarity up the surface of the wafer. The contact line between the liquid and the solid is rough, displaying a 0.3 mm root-mean-square deviation from straight and a 1 cm wavelength parallel to the front. The roughness is worse when Photoflow is not added to the wa-

 ©2003 The American Physical Society

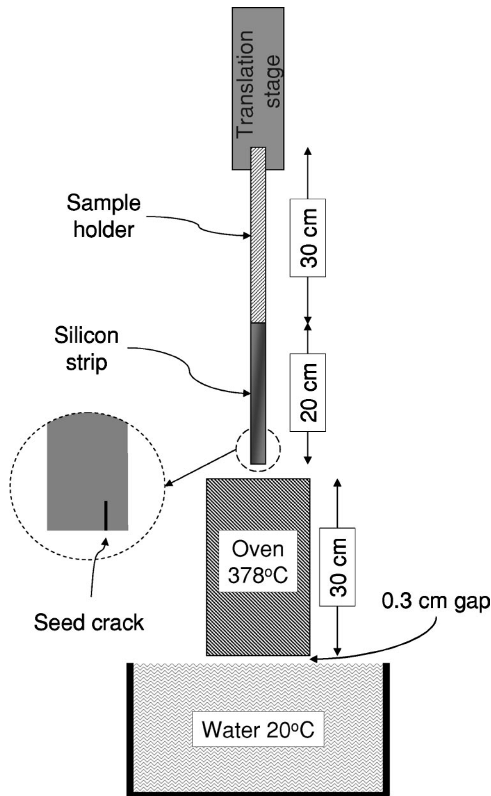

FIG. 1. Schematic of experimental setup. A rectangular strip of single-crystal silicon is attached to a translation stage by a long, thin, ceramic sample holder. The sample is seeded with a crack approximately one-quarter of the sample's width from the edge. The translation stage is driven by a microstepping motor. The silicon sample is lowered into the oven, allowed to equilibrate to the oven temperature, and then plunged into the water bath at a constant rate. A crack initiates from the notch. Depending on the lowering speed the crack can be straight or wavy, or bifurcated with two or more straight or wavy branches.

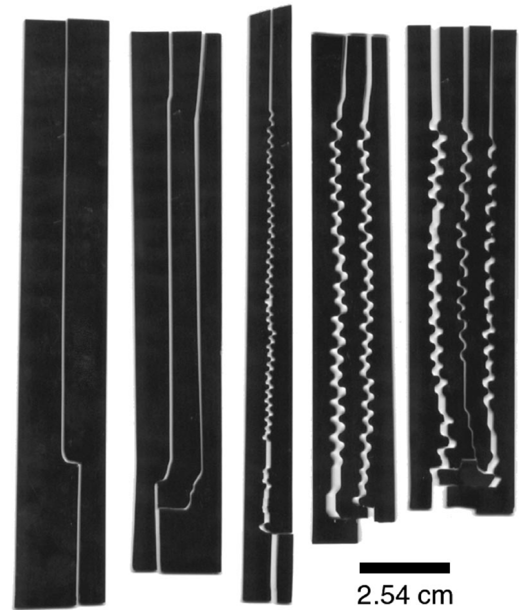

FIG. 2. Fractured samples. The fragments have been separated to show the path of the crack. The cracks ran from bottom to top. The samples show, from left to right, a single straight crack (width $w=2.4$ cm and speed $v=0.4$ cm/s), a double straight crack ($w=2.4$ cm and $v=1.1$ cm/s), a single wavy crack ($w=1.2$ cm and $v=3.0$ cm/s), a double wavy crack ($w=1.9$ cm and $v=2.6$ cm/s), and a triple wavy crack ($w=2.6$ cm and $v=2.8$ cm/s).

ter. Cleaning the sample with a piranha solution (3 parts H_2SO_4 to 1 part H_2O_3) does not affect the roughness; heating the sample appears to nullify the benefits of cleaning. The crack tip runs approximately 5 mm above the water surface, and it draws water up its length by capillarity. Numerous samples with widths w ranging from 1.0 to 3.5 cm have been run at a constant dipping speed v ranging from 0.5 to 6.0 cm/s.

III. RESULTS

Depending on the width and dipping speed, we observe single straight or wavy cracks, or multiply branched cracks with wavy or straight branches (see Fig. 2). Multibranched cracks result from a bifurcation of a single initial crack. Most often the branches of a multibranched fracture are either all straight or all wavy; occasionally, in a single sample some branches are wavy and others are straight. In all cases, the

TABLE I. Properties of silicon.

Property	Symbol	Value	Units	Temperature	Reference
Density	ρ	2.329×10^3	kg/m^3	20–400 °C	[11]
Young's modulus	$E(110)$	171	GPa	20–400 °C	[12]
Surface energy	$\gamma_{\langle 110\rangle}$	2.6	J/m^2	20–400 °C	[12]
Thermal expansion coefficient	α_T	2.6×10^{-6}	K^{-1}	20 °C	[13]
		3.8×10^{-6}	K^{-1}	378 °C	[13]
Specific heat	C_p	694	J/kg K	20 °C	[13]
		800	J/kg K	378 °C	[13]
Thermal conductivity	κ	157	W/m K	20 °C	[13]
		50.0	W/m K	378 °C	[13]
Thermal diffusivity	$D=\frac{\kappa}{C_p\rho}$	9.7×10^{-5}	m^2/s	20 °C	
		2.7×10^{-5}	m^2/s	378 °C	

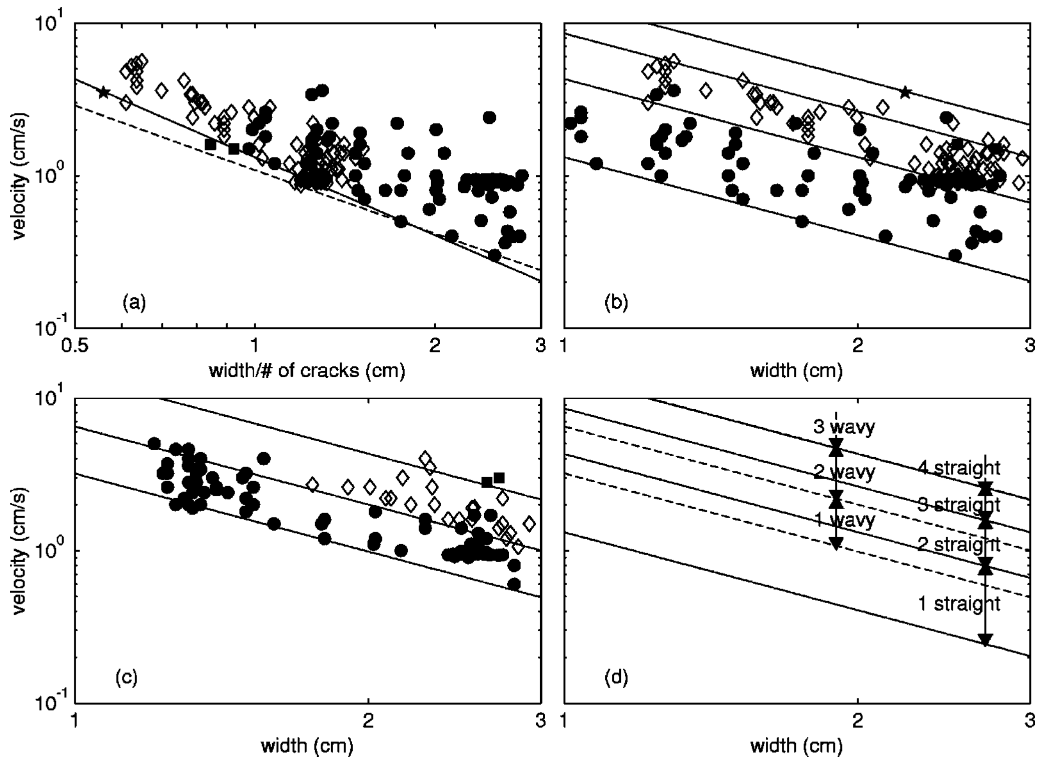

FIG. 3. Crack mode dependence on velocity v and width w. (a) Runs that yielded one or more straight cracks, plotted as a function of width of the original sample divided by the number of cracks. The symbols ●, ◇, ■, and ⋆ correspond, respectively, to single, double, triple, and quadruple cracks. The solid line shows our estimate of the boundary between no cracks and straight cracks, $v=Aw^{-1.7}$. The dashed line is the predicted boundary from the thermoelastic calculation of Marder [2], Eq. (2). (b) The same data as (a) but without dividing by the number of cracks. The solid lines are the unscaled versions of the boundary curve in (a). (c) Runs that yielded a wavy crack. The symbols ●, ◇, and ■ correspond, respectively, to single, double, and triple wavy cracks. The solid lines represent our estimate of the transition boundary between the n and $n+1$ wavy crack, again $v=Aw^{-1.7}$. (d) Depiction of the full phase portrait. The solid lines correspond to the boundary lines in (b) and the dashed lines correspond to the boundary lines in (c).

branches ran parallel and equidistant from their neighbors. We observed as many as four branches.

The experimentally observed fracture mode as a function of speed and sample width is shown in the four panels of Fig. 3. Figure 3(a) shows data for straight cracks as a function of v and w/n where n is the number of branches. Cracks appear

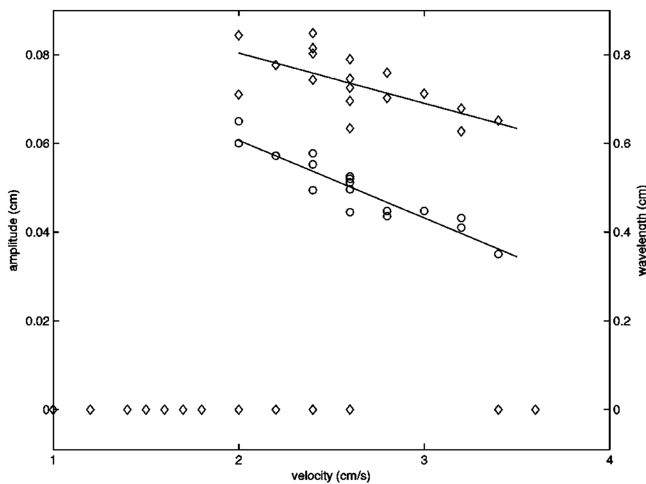

FIG. 4. Wavelength and amplitude of the oscillations as a function of velocity for samples with $w=1.39\pm0.05$ cm.

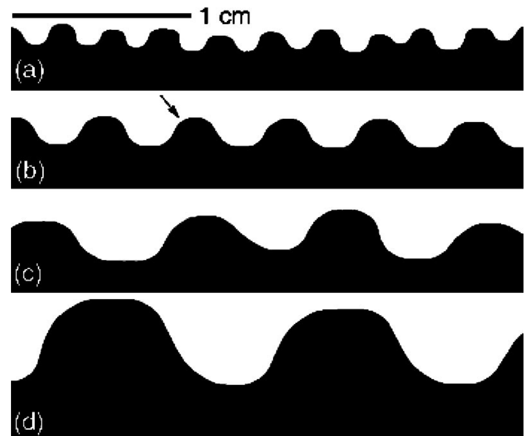

FIG. 5. Photographs of samples with a single wavy crack, representative of the observed range of amplitude and wavelength. Only one-half of each sample is shown. The crack traveled from left to right. These samples were made with (a) width $w=1.3$ cm and speed $v=5.0$ cm/s, (b) $w=1.3$ cm and $v=2.0$ cm/s, (c) $w=2.5$ cm and $v=1.7$ cm/s, and (d) $w=2.5$ cm and $v=0.9$ cm/s. The arrow on (b) indicates the approximate location of the AFM scans discussed below.

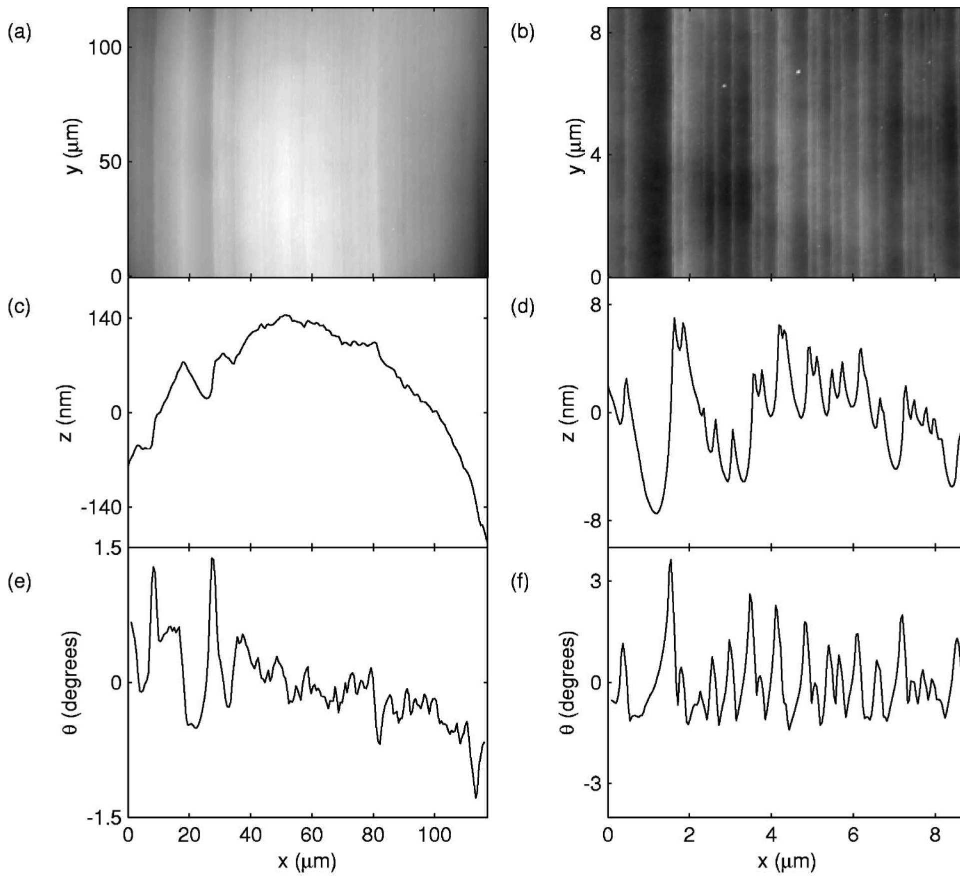

FIG. 6. AFM micrograph of fracture surface of wavy crack from a single run and derived data. (a),(b) AFM images of the same fracture surface at two different levels of magnification. (c),(d) Profiles from (a),(b), respectively, obtained by averaging over the y direction. (e),(f) Angle with respect to the x axis of the tangent to the surface profiles in (c),(d). Note that the vertical scales in (c),(d) are expanded compared with the corresponding horizontal scales, in order to show the features clearly.

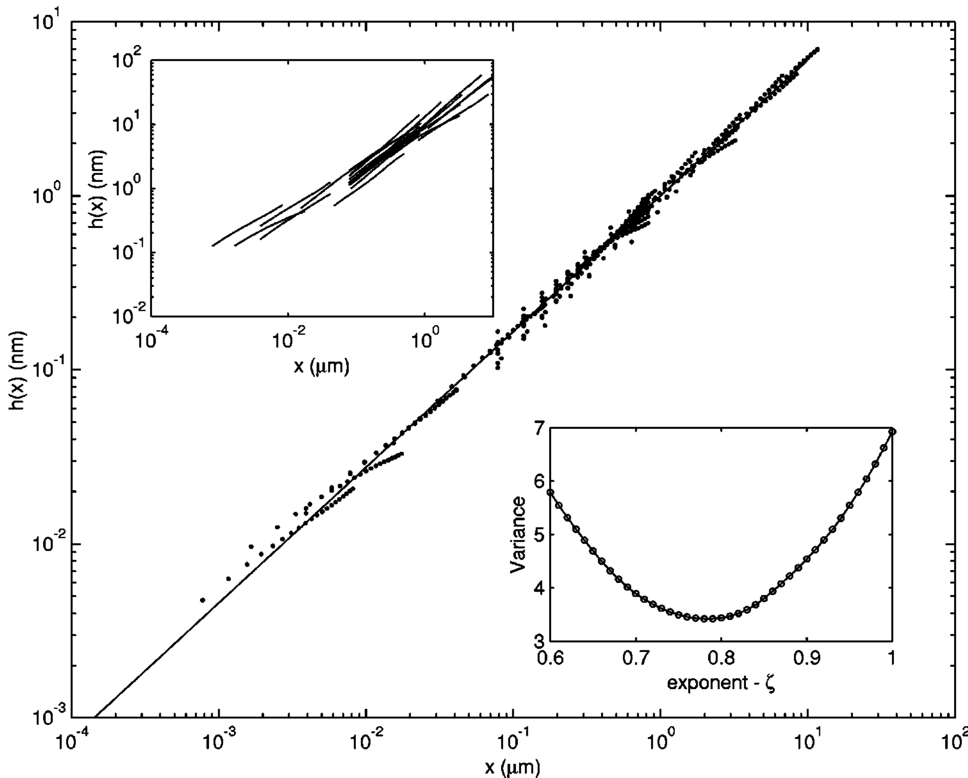

FIG. 7. Height fluctuation $h(x)$ versus window size x. The solid line shows a power law fit to the data that gives an exponent $\zeta = 0.78 \pm 0.07$. The data from each image have been shifted by assuming a power law behavior, finding the unique exponent that minimizes the sum of the variations of the fit to the power law (see inset), and dividing through by the prefactor obtained in the previous step. The variation of the prefactor is due to the statistical fluctuation of a small data set.

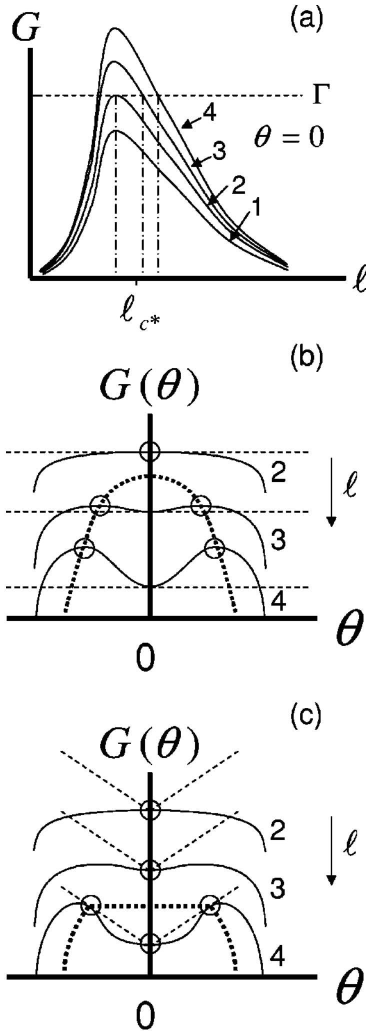

FIG. 8. Heuristic model of subcritical transition. (a) Schematic of energy release rate for a straight crack in a nonlinear temperature gradient as a function of crack length ℓ above the water bath for four different loadings, increasing from 1 through 4. The dashed horizonal line is the surface energy and the intersection of the energy release rate and this line sets the length of crack above the water. For $\ell \geqslant \ell_c$ a straight crack in an isotropic material is no longer stable and it will begin to oscillate. (b) Schematic of the angular dependence of G where θ is the angle away from the line of symmetry. The horizontal dashed line shows the angular dependence of the surface energy, or rather lack of it, for an isotropic solid. In this figure a change in the loading is shown as a downward shift of the surface energy. The ○ represent attractors. For loading 3, $\ell > \ell_c$, the excess of G over Γ represents excess kinetic energy that will drive the crack off axis, and the attractor moves off axis. The dotted curve indicates the bifurcation diagram. (c) Schematic of the angular dependence of G where θ is the angle away from the line of symmetry, identical to that shown in (b). Again, increased loading is represented by the downward shift of the surface energy. However, in contrast to an isotropic solid, the surface energy for a crystal has a strong angular dependence with a discontinuous slope. While loading 3 would lead to an oscillating crack in an isotropic solid, there is sufficient energy for a crack to travel off axis in a crystal. Therefore, the transition point to a wavy crack is postponed until the loading reaches case 4, where Γ just touches G at a finite θ.

only in the portion of parameter space above the solid line. The solid line is a fit to a power law and yields $v = Aw^{-1.7}$ with $A = 1.3\ \mathrm{cm}^{2.7}/\mathrm{s}$. Hence, to initiate n straight parallel cracks the sample must be lowered at $v \geqslant A(w/n)^{2.7}$.

The data from panel (a) are reproduced in (b) without the scaling by the number of branches; the boundaries as determined above are plotted as solid lines. The data show that n straight parallel cracks are stable only in a limited region of parameter space. Thus, for fixed width and increasing velocity there is a series of transitions from n to $n+1$ straight parallel cracks with $n = 0, \ldots, 3$.

Scaling the data for wavy cracks by the number of branches does not result in a single boundary for initiation as it does in the case of straight cracks. Panel (c) shows data for wavy cracks as a function of v and w. These data also appear to segregate into mutually exclusive regions. With the power law function obtained from the fit to panel (a), the boundary between n wavy cracks and $n+1$ wavy cracks has been chosen by eye.

Panel (d) shows only the boundaries obtained from the data in (b) and (c) to illustrate the overlap of the wavy and straight regions. The overlap seen in Fig. 3(d) indicates that the fracture mode can be either straight or wavy for the same parameter values. This is further illustrated by Fig. 4, where the amplitude of oscillation of a single wavy crack exhibits two branches. The zero amplitude branch corresponds to straight cracks, and the nonzero amplitude branch corresponds to oscillating cracks. The overlap of these branches demonstrates the system's bistability. We have not been able to map out the attractor basin for each of the states, and thus we are unable to determine if the wavy state is an analytic continuation of the straight state.

Given the strong preference for $\langle 100 \rangle$ wafers to cleave along $\langle 110 \rangle$ surfaces, the wavy crack profiles are surprisingly smooth (see Fig. 5). However, an optical microscope reveals that there are striations perpendicular to the direction of crack motion that span the thickness of the sample. We measured these striations in a small region on a single sample using an atomic force microscope (AFM), expecting to find a staircase structure tied to the $\langle 110 \rangle$ planes. We used a commercial AFM manufactured by Digital Instruments to scan sections of the surface from 140 μm down to 500 nm with a horizontal resolution of 2 nm and vertical resolution of 1 nm. The scans are taken from a portion of the surface that is approximately 30° off from the $\langle 110 \rangle$ directions, as indicated in Fig. 5. Instead of the expected staircase, we find [see Figs. 6(c) and 6(d)] that the surfaces display no obvious faceting. Furthermore, the AFM scans reveal that the striations exist on all length scales down to the limit of our resolution. Indeed, the surface is self-affine, $Z(x,y) = \lambda^{\zeta} Z(\lambda x, y)$, as is shown by the following computation. Each image yields a height map of the surface $Z_i(x,y)$, where i is the image number. We extract a single profile $z_i(x)$ from Z_i. A calculation of the height fluctuations $h(x)$ in a window of size x [16],

$$h_i(x) = \langle \max[z_i(\tilde{x})]_{\tilde{x} \in [x_0, x_0+x]} - \min[z_i(\tilde{x})]_{\tilde{x} \in [x_0, x_0+x]} \rangle_{x_0}, \tag{1}$$

where x is limited to half the image size, yields the data in the upper inset of Fig. 7. Each image yields a power law dependence of $h_i(x) \sim x^{\zeta}$ although the prefactors of different images are not equal. The "best" exponent has been determined by the following algorithm: (1) the exponent ζ is fixed and the best prefactor $b_i = \langle h_i(x)/x^{\zeta} \rangle$ is computed for each data set; (2) the variance $\sigma_i = \sqrt{\Sigma_j \{\log_{10}[h_i(x_j)] - \log_{10}(b_i x_j^{\zeta})\}^2}$ is computed for each data set and the result summed over i to yield $\sigma(\zeta)$; (3) the calculation of $\sigma(\zeta)$ is repeated for several values of ζ on the interval [0.5,1] and the best exponent is chosen as the value of ζ that minimizes $\sigma(\zeta)$ (see lower inset in Fig. 7). This procedure yields $\zeta = 0.78 \pm 0.07$ where the error bars reflect statistical error as opposed to systematic variations that may arise from our methodology [14]. The main result is the rescaled data in Fig. 7, which show scaling over three decades of length. Similar results were obtained when the wafer was chemically polished on both sides and when the size of the steps on the stepper motor was changed.

IV. DISCUSSION

Our observations reveal three results: the initiation point for straight multibranched cracks scales as $v(n/w)^{1.7}$, the transition from straight to wavy cracks is discontinuous and bistable, and the surface of a wavy crack is self-affine along the direction of crack motion (there is no indication of cleavage planes). Here we consider these results.

The energy released per unit length increase of the crack, G, is a single-peaked function of the crack length above the water bath, ℓ. G is proportional to the stress squared, the stress is proportional to d^2T/dx^2, and thus $G \propto (d^2T/dx^2)^2$. The temperature is low in the water bath and high in the oven, and because the temperature is set by diffusion it rises monotonically from low to high. The second derivative of T is thus a function with a single maximum which dictates that G too has a single maximum. As the forcing parameters (v, w, or δT) increase, the maximum grows until it is equal to the energy needed to create two units of new surface area Γ. At this point, known as the Griffith point [15], crack propagation is energetically favorable.

The analysis of Marder [2] showed that for a single straight crack

$$G = \frac{1}{2}(1-\nu^2)Ew(\alpha_T \Delta T)^2 K^2, \tag{2}$$

where ν is the Poisson ratio, E is the Young's modulus, α_T is the coefficient of thermal expansion, ΔT is the temperature difference between the oven and the water, D is the thermal diffusivity, and K is a dimensionless function of the dimensionless parameter group $v\ell/D$. Griffith's criterion gives $G(\ell_m) = 2\gamma_{\langle 110 \rangle}$ where $\gamma_{\langle 110 \rangle}$ is the surface energy of a $\langle 110 \rangle$ facet and ℓ_m is the value of ℓ that maximizes G. Combining Eq. (2) with the Griffith criterion and collecting constants gives $\gamma_{\langle 110 \rangle} = Cwf(v)$ at the crack initiation point and $v \sim f^{-1}(w)$. Our results show that $f^{-1}(w) = w^{-1.7}$.

Using the values in Table I, we obtain from Eq. (2) the dashed line in Fig. 3(a). The line systematically deviates from the data but is a reasonable estimate of the boundary, given the assumptions of temperature independent material parameters and an overly simplistic temperature profile.

If we assume that the energy release rates for each crack in a multibranched fracture are equal and are of the same form as a single crack, then Griffith's criterion gives $\gamma_{\langle 110 \rangle} = C(w/n)f(v)$, and it follows as above that $v \sim f^{-1}(w/n)$. This reasonable guess agrees with the experimental results.

When cracks in glass are driven beyond the point where straight motion becomes unstable, wavy cracks grow continuously in amplitude as the speed increases [1]. In silicon, we never observe wavy cracks of small amplitude; the transition from straight to wavy cracks is discontinuous and hysteretic. We can explain this observation qualitatively if we recall that the energy needed to form a new surface in a crystal has a cusplike minimum as a function of angle around directions corresponding to preferred fracture planes.

Consider the curves in Fig. 8(a) representing the ℓ dependence of G for four different loadings. The Griffith point is found where Γ and G intersect. When the peak of G is less than Γ, as in case 1, there is no such point and therefore no crack propagation. Case 2 represents the minimum loading need for a crack to propagate. For curves 3 and 4 there are two such intersections but only the solution to the right of the peak is stable.

Adda-Bedia and Pomeau [3] showed for an isotropic solid that ℓ is set by the relation $G(\ell) = \Gamma$ and there exists a critical length ℓ_c beyond which a straight crack loses stability to a wavy crack in a continuous manner. This is illustrated pictorially in Fig. 8(b), which shows the angular dependence of $G(\theta)$ as experienced by an initially straight crack. The dashed line is $\Gamma(\theta)$, which is constant because the solid is isotropic; instead of shifting $G(\theta)$ up when the loading changes we instead shift Γ down. The ○ represent attractors in the dynamical systems sense. For low loading $\ell < \ell_c$ and G is peaked at $\theta = 0$, and so the attractor is at $\theta = 0$. As the loading increases ℓ exceeds ℓ_c and the attractor bifurcates and moves continuously off the $\theta = 0$ line. The bifurcation diagram for this transition is shown as the dotted curve.

For a crystalline solid $\Gamma(\theta)$ is no longer constant, and it should have a cusp as θ moves away from a preferred fracture direction. This situation is depicted in Fig. 8(c). The dashed curve is $\Gamma(\theta)$ and again it is shifted downward as the loading increases. Unlike the behavior of the crack in an isotropic solid, the attractor remains at $\theta = 0$ for case 3 because $\Gamma(\theta) > G(\theta)$ for all θ. As the loading increases further, case 4 is reached, at which point attractors appear at finite values of θ. An attractor remains on the $\theta = 0$ line so the system is bistable.

Since the bistability and hysteresis in crack motion are so naturally explained by invoking the strong tendency to move along fracture planes, the failure of wavy cracks to exhibit facets is surprising. Observing that the crack surfaces are self–affine is also surprising because the leading theory for fracture surface roughness ascribes this property to pinning by defects. However, semiconductor grade silicon is as near perfect a crystal as can be made. Contrast silicon wafers, which are free of dislocations and inclusions, monocrystalline, and exceedingly pure with at most 10^{18} dissolved im-

purities per cm^3 (about $10^{-3}\%$), with a typical metallic alloy, which has 10^{15} dislocation lines per cm^2, grain boundaries of size 1 μm, and impurities on the order of $10^{-1}\%$ which often form inclusions. Yet, aside from the anisotropy of the fractal scaling in silicon there is no obvious difference between fractal scaling of silicon and alloys [16]—the scaling range is similar and the roughness exponent is the same.

It is conceivable that the contact line, because of its roughness or its stick slip motion, the pits and grooves on the mechanically polished side of the wafer, or the steplike motion of the stepper motor produces a fluctuating force on the crack front. However, we find that using a double-side polished wafer or different stepping sizes on the motor does not change the surface roughness. In addition, the roughness of the contact line seems an unlikely source of noise since St. Venant's principle dictates that the distortions of the stress field will decay on distances comparable to the size of the perturbation, which is much shorter than the distance of the crack tip from the water surface. We cannot exclude all the sources of random forcing. For example, other sources of noise that we have not considered are the roughness of a chemically polished wafer, lattice trapping [17], or evaporation of fluid sucked by capillarity into the crack.

Irrespective of the source of noise, any theory that purports to explain the roughness of the fracture surface in silicon must contend with the translational invariance along the crack front that is demonstrated by the lack of roughness across the width of the fracture surface. Theories that yield a roughness exponent of 0.8 require roughness in the transverse direction too.

V. CONCLUSIONS

We have shown that cracks in single-crystal silicon display the same hierarchy of transitions observed in an isotropic solid when subjected to the same thermal loading conditions; we observed, with increasing load, transitions from straight to wavy to multiply branched cracks. We also found that the anisotropic fracture energy suppresses the onset of these transitions and that the transitions are discontinuous, bistable, and hysteretic.

In addition, we found that cracks that deviate from the preferred $\langle 110 \rangle$ plane can travel in arbitrary directions. Furthermore, the direction of the crack fluctuates wildly, creating a fractal fracture surface with a roughness exponent of 0.8, equal to that seen in highly heterogenous materials.

ACKNOWLEDGMENTS

We gratefully acknowledge the donation of wafers by Silicon Genesis Incorporated and MEMC. We thank William D. McCormick and Eran Sharon for valuable discussions and Paul Petersan for assistance with the experiment. This work was supported by NSF under Grants No. DMR 9802562 and No. DMR 0072834.

[1] A. Yuse and M. Sano, Nature (London) **362**, 329 (1993).
[2] M. Marder, Phys. Rev. E **49**, R51 (1994).
[3] M. Adda-Bedia and Y. Pomeau, Phys. Rev. E **52**, 4105 (1995).
[4] B. Yang and K. Ravi-Chandar, J. Mech. Phys. Solids **49**, 91 (2001).
[5] O. Ronsin, F. Heslot, and B. Perrin, Phys. Rev. Lett. **75**, 2352 (1995).
[6] A. Yuse and M. Sano, Physica D **108**, 365 (1997).
[7] O. Ronsin and B. Perrin, Europhys. Lett. **38**, 435 (1997).
[8] O. Ronsin and B. Perrin, Phys. Rev. E **58**, 7878 (1998).
[9] R. V. Goldstein and R. L. Salganik, Int. J. Fract. **10**, 507 (1974).
[10] B. D. Ferney, M. R. DeVary, K. J. Hsia, and A. Needleman, [Scr. Mater. **41**, 275 (1999)] report wavy cracks in silicon but give no details.
[11] H. F. Wolf, *Silicon Semiconductor Data* (Pergamon Press, Oxford, 1969).
[12] C. P. Chen and M. H. Leipold, Am. Ceram. Soc. Bull. **59**, 469 (1980).
[13] Y. S. Touloukian and E. H. Buyco, *Themophysical Properties of Matter* (IFI/Plenum, New York, 1970).
[14] J. Schmittbuhl, J. P. Vilotte, and S. Roux, Phys. Rev. E **51**, 131 (1995).
[15] B. Lawn, *Fracture of Brittle Solids*, 2nd ed. (Cambridge University Press, Cambridge, 1993).
[16] E. Bouchaud, J. Phys.: Condens. Matter **9**, 4319 (1997), and references therein.
[17] R. Thomson, C. Hseih, and V. Rana, J. Appl. Phys. **42**(8), 3154 (1971).